Extended Parallel Backprojection (EPBP) for Arbitrary Cone Angle and Arbitrary Pitch 3D and Phase–Correlated 4D CT Reconstruction

Marc Kachelrieß*, Willi Kalender

Abstract— **Recent developments in medical CT aim at faster rotation speeds and a higher number of simultaneously acquired slices. These efforts are pushed further by cardiac CT which is currently the most prominent special–purpose application in CT [1]. Today, 16-slice scanners are state–of–the–art. But CT manufacturers have already announced scanners with far more slices and some even promote prototypes with up to 256 slices.**

Medical CT must support the circular scan trajectory (sequence scan) and the spiral trajectory (spiral scan). Arbitrary pitch selection is of high importance. In any case, the complete area of the detector is to be exposed and each measured ray should contribute to the image. Only then, optimized dose usage can be achieved.

These requirements cannot be fulfilled by current reconstruction approaches. Exact cone–beam reconstruction, that is capable of reconstructing large cone–angle data, cannot cope with arbitrary pitch and phase–correlated data segments. Only approximate reconstruction approaches have the potential to handle all requirements. Currently, the only known approach that can handle phase–correlated true cone–beam data is an extension to the Advanced Single–Slice Rebinning (ASSR) algorithm [2], [3]. However, this generalized approach ASSR CI is limited to 32 slices.

We have therefore developed a new approximate Feldkamp–type algorithm, the extended parallel backprojection (EPBP)[4]. Its main features are a phase–weighted backprojection and a voxel–by–voxel 180° normalization. The first feature ensures 3D and 4D capabilities with one and the same algorithm, the second ensures 100% detector usage (each ray counts!). The algorithm is evaluated using simulated data of a thorax phantom and a cardiac motion phantom for scanners with up to 256 slices.

The standard reconstructions (EPBP Std) are of excellent quality even for as many as 256 slices. The cardiac reconstructions (EPBP CI) are of high quality as well and show no significant deterioration of objects even far off the center of rotation. Since EPBP CI uses the cardio interpolation (CI) phase weighting the temporal resolution is equivalent to that of the well known single–slice and multi–slice cardiac approaches 180°CI, 180°MCI, and ASSR CI, respectively, and lies in the order of 50 ms to 100 ms for rotation times between 0.4 s and 0.5 s.

I. Introduction

MEDICAL computed tomography is currently evolving faster than ever. Increased spatial resolution, decreased scan time, increased temporal resolution, decreased patient dose, and increased volume coverage are some of the important trends to mention.

As little as five years ago, single–slice spiral CT was the state–of–the–art. Then, the first 4–slice scanners became available. Already in 2001, 16–slice scanners started to replace the 4–slice machines. Apparently, the near future will shift the number of simultaneously scanned slices to 32, 64 and even more. Slice thickness, and thereby spatial resolution, will continue to decrease to further improve diagnostic accuracy. At the same time, dose utilization will increase to keep the effective patient dose at an acceptable level: dose modulation techniques, automatic exposure control and improved detector materials will help to do so [1].

Besides improved spatial resolution, improved contrast resolution and low patient dose one is further interested in highest temporal resolution to allow imaging the heart. This is done using short rotation times combined with dedicated phase–correlated reconstruction algorithms as they are available since 1996/1997 [5].

The relevance for image reconstruction algorithms lies in the expected increase in cone angle and in the demand for phase–correlated reconstruction. Neglecting the cone–angle of the scanner as done in all 4–slice and in all commercial *cardiac* 16–slice reconstruction algorithms will yield unacceptable image artifacts for future scanners.

There are fast and efficient cone–beam algorithms with acceptable image quality available for cone–beam spiral CT. However, they do not ensure 100% dose usage and/or they do not work for arbitrary spiral pitch. Further, none of them is capable of combining these demands with phase–correlated imaging at wider cone angles.

To fill the missing gap, we propose EPBP, a new approximate cone–beam reconstruction that allows for arbitrary pitch and for phase–correlated reconstruction and that ensures 100% detector usage. Details of cardiac CT scanning and the restrictions on the maximum pitch as a function of the patient's heart rate can be found in references [6], [7], [8]. The phase selection mechanisms described there, namely the cardio interpolation (CI) and the cardio delta (CD) approach are used for EPBP as well. Especially EPBP CI that uses CI, the most promising multi–phase weighting currently available, is evaluated here.

In this paper, we will outline the EPBP Std and the EPBP CI algorithm and give some descriptive examples.

II. Simulations

To evaluate our new approach we have simulated spiral cone–beam data corresponding to the in–plane geometry of a typical medical CT scanner (1160 projections per rotation, 672 detector channels per detector row, and a fan angle $\Phi = 52°$) using a dedicated x–ray simulation tool (ImpactSim, VAMP GmbH, Möhrendorf, Germany). Two

Institute of Medical Physics, University of Erlangen–Nürnberg, Krankenhausstr. 12, 91054 Erlangen. Corresponding author: PD Dr. Marc Kachelrieß, E–mail: marc.kachelriess@imp.uni–erlangen.de

phantoms have been simulated: the thorax phantom described in the phantom data base http://www.imp.uni–erlangen.de/forbild and the cardiac motion phantom described in [7].

The simulated scan protocol uses 0.42 s rotation time (143 rpm), $M \times 0.75$ mm collimation with $M = 2^m$ simultaneously scanned slices where $m = 4, \ldots, 8$, and a pitch of $p = 0.375$. The table increment can be found as $d = MSp$.

III. Geometry

A. Scan Geometry

The scan geometry assumed here is a fan–beam geometry with cylindrical detectors and a spiral focus trajectory. The EPBP approach is based on a rebinning to parallel geometry. Other geometries, such as flat detectors, can be easily incorporated by modifying the corresponding rebinning and transform equations. Note that in the limit of $p = 0$, the spiral reduces to a circular trajectory. EPBP copes with sequence data as well as it does with spiral data.

The source trajectory is parameterized by the view angle α as

$$\boldsymbol{s}(\alpha) = R_{\mathrm{F}} \begin{pmatrix} \sin\alpha \\ -\cos\alpha \\ 0 \end{pmatrix} + d \begin{pmatrix} 0 \\ 0 \\ 1 \end{pmatrix} \frac{\alpha}{2\pi}. \tag{1}$$

R_{F} denotes the radius of the focal spot trajectory and d denotes the table increment per rotation.

The coordinate vector of the detector element (α, β, b) is given as

$$\boldsymbol{r}(\alpha,\beta,b) = \boldsymbol{s}(\alpha) + R_{\mathrm{FD}} \begin{pmatrix} -\sin(\alpha+\beta) \\ \cos(\alpha+\beta) \\ 0 \end{pmatrix} + b \begin{pmatrix} 0 \\ 0 \\ 1 \end{pmatrix};$$

β and b denote the transaxial and longitudinal detector components, respectively.

To rebin the transaxial components of the cone–beam data to parallel geometry we parameterize a ray by its distance ξ to the axis of rotation and by its angle ϑ with respect to the negative y–axis. The normal form of the ray's x–y–components is given as $x\cos\vartheta + y\sin\vartheta - \xi = 0$. This definition was chosen to have the central rays for fan–beam ($\beta = 0$) and for parallel beam ($\xi = 0$) coinciding for $\alpha = \vartheta$. The relation between a ray in fan–beam coordinates (α, β) and a parallel–beam ray (ϑ, ξ) is the familiar transform

$$\begin{aligned} \vartheta &= \alpha + \beta \\ \xi &= -R_{\mathrm{F}} \sin\beta \end{aligned} \quad \text{and} \quad \begin{aligned} \alpha &= \vartheta + \arcsin\xi/R_{\mathrm{F}} \\ \beta &= -\arcsin\xi/R_{\mathrm{F}} \end{aligned}. \tag{2}$$

B. Point Projection

For backprojection, we need to know the detector coordinates (ξ, b) that result from projecting the point (x, y, z) from $\boldsymbol{s}(\alpha)$ onto the cylindrical detector. The radial coordinate is given as

$$\xi = x\cos\vartheta + y\sin\vartheta.$$

The longitudinal detector coordinate can be computed using the intersection theorem. The transaxial distance of the respective voxel to the source is given as

$$\begin{aligned} D^2 &= (R_{\mathrm{F}}\sin\alpha - x)^2 + (R_{\mathrm{F}}\cos\alpha + y)^2 \\ &= R_{\mathrm{F}}^2 - 2R_{\mathrm{F}} r \sin(\alpha - \varphi) + r^2 \end{aligned}$$

with $(x, y) = (r\cos\varphi, r\sin\varphi)$ or, equivalently,

$$D = R_{\mathrm{F}}\cos\beta + \eta = \sqrt{R_{\mathrm{F}}^2 - \xi^2} + \eta$$

with $\eta = y\cos\vartheta - x\sin\vartheta$. Now, find b by scaling the axial distance $z - d\frac{\alpha}{2\pi}$ from D to R_{FD}:

$$b = \frac{R_{\mathrm{FD}}}{D}(z - d\frac{\alpha}{2\pi}). \tag{3a}$$

And we find another representation of ξ:

$$\xi = -R_{\mathrm{F}}\sin\beta = R_{\mathrm{F}}\frac{x\cos\alpha + y\sin\alpha}{D}. \tag{3b}$$

IV. Reconstruction

The extended parallel backprojection algorithm consists of the following five steps:

- azimuthal rebinning: $p(\alpha,\beta,b) \to p(\vartheta,\beta,b)$,
- longitudinal rebinning: $p(\vartheta,\beta,b) \to p(\vartheta,\beta,l)$,
- radial rebinning: $p(\vartheta,\beta,l) \to p(\vartheta,\xi,l)$,
- convolution: $p(\vartheta,\xi,l) \to \hat{p}(\vartheta,\xi,l)$,
- weighting and backprojection: $\hat{p}(\vartheta,\xi,l) \to f(x,y,z)$.

A. Azimuthal Rebinning

The original projection data $p(\alpha,\beta,b)$ are converted from fan–beam to fan–parallel geometry using (2) as follows:

$$p(\vartheta,\beta,b) = p(\alpha,\beta,b) \quad \text{with} \quad \alpha = \vartheta - \beta.$$

B. Longitudinal Rebinning

Convolving spiral data in the detector row direction (constant b) yields severe cone–beam artifacts. As indicated by ASSR [2], SMPR [9], and exact cone–beam reconstruction [10] the optimal direction of convolution is the tangent $d\boldsymbol{s}(\alpha)/d\alpha$. To align the fan–parallel detector rows with the optimal direction of convolution a longitudinal rebinning is required. Therefore, we are interested in the relationship between b and ξ when moving along $d\boldsymbol{s}$. Using (3) one finds

$$\frac{db}{d\xi} = \frac{d(bD)}{d(\xi D)} = \frac{R_{\mathrm{FD}}\,dz}{R_{\mathrm{F}}(dx\cos\alpha + dy\sin\alpha)} = \frac{R_{\mathrm{FD}}\,d}{2\pi\,R_{\mathrm{F}}^2};$$

in the last step (1) was used to insert the components of $d\boldsymbol{s}$. Now, we define a new longitudinal variable l as

$$b = l + \lambda\xi \quad \text{with} \quad \lambda = \frac{db}{d\xi} = \frac{dR_{\mathrm{FD}}}{2\pi\,R_{\mathrm{F}}^2}$$

such that $dl/d\xi = 0$ in the direction of $d\boldsymbol{s}$. Then, do the longitudinal rebinning

$$p(\vartheta,\beta,l) = p(\vartheta,\beta,b) \quad \text{with} \quad b = l + \lambda\xi = l - \lambda R_{\mathrm{F}}\sin\beta$$

to switch to l as the new independent variable.

Whenever b exceeds the detector limits $b_{\min}$ and $b_{\max}$ for some β we extrapolate by repeating the outermost detector row. The values that are made up by extrapolation are required during convolution which operates on complete detector rows, always. During backprojection these extrapolated points are *not* accessed; backprojection rather respects the physical detector area!

C. Radial Rebinning

The radial rebinning converts to equidistant parallel coordinates. We use (2) to find

$$p(\vartheta, \xi, l) = p(\vartheta, \beta, l) \quad \text{with} \quad \beta = -\arcsin \xi / R_{\mathrm{F}}.$$

D. Convolution

Now, convolution of the detector rows is performed using a standard convolution kernel $k(\xi)$, as, for example, the Shepp–Logan kernel.

$$\hat{p}(\vartheta, \xi, l) = p(\vartheta, \xi, l) * k(\xi)$$

yields the convolved data $\hat{p}$ needed for backprojection.

E. Weighting and Backprojection

In this step, we regard the backprojection of a fixed voxel, say one located at $\boldsymbol{r} = (x, y, z)$. Let V denote the set of view angles ϑ under which $\boldsymbol{r}$ is measured.

Assume a temporal window T that comprises all ϑ that correspond to *allowed data*. For the standard reconstruction EPBP Std, all data acquired are allowed data and therefore $T = \mathbb{R}$. For the reconstruction of cardiac data, T can be defined by specifying a cardiac motion phase c_{R} that counts relative to some synchronization peaks and a phase width $0 < \Delta c \leq 1$; T will then consist of a set of disjunct intervals. EPBP CI chooses Δc as small as allowed by the completeness condition (see below). Other definitions may include absolute timing information or the restriction to only one temporal interval of length π (single–phase reconstruction), or two intervals (bi–phase reconstruction).

Regardless of what convention is used to define T, the intersection $I = V \cap T$, that comprises all views to be used, must be 180°–complete:

$$\bigcup_k (I + k\pi) = \mathbb{R}.$$

Now, assume a weighting function $w(\vartheta)$ whose support equals I, i.e. $w(\mathbb{R} \setminus I) = \{0\}$, and $\sum_k w(\vartheta + k\pi) \neq 0$. The last condition can easily be achieved by using positive weights on I only. For EPBP CI we use a multi–triangular weight function: triangle functions located on each of I's disjunct intervals.

By normalizing w as

$$\hat{w}(\vartheta) = \frac{w(\vartheta)}{\sum_k w(\vartheta + k\pi)}$$

we achieve

$$\sum_k \hat{w}(\vartheta + k\pi) = 1 \quad \text{and} \quad \int d\vartheta\, \hat{w}(\vartheta) = \pi.$$

Backprojection

$$f(x, y, z) = \int d\vartheta\, \hat{p}(\vartheta, \xi, l) \hat{w}(\vartheta)$$

with

$$\xi = \xi(x, y, \vartheta) = x \cos\vartheta + y \sin\vartheta$$
$$\alpha = \vartheta - \beta = \vartheta + \arcsin \xi / R_{\mathrm{F}}$$
$$l = b(x, y, z, \alpha) - \lambda \xi$$

then yields the desired voxel value at (x, y, z).

V. Results

Figure 1 shows that image quality of the thorax phantom is excellent with EPBP, even for as many as 256 slices. As indicated by the ribs, ASSR (which is in fact designed for up to about only 60 slices [2]) cannot cope with this large cone–angle; the same applies to the highly related AMPR algorithm defined in reference [11].

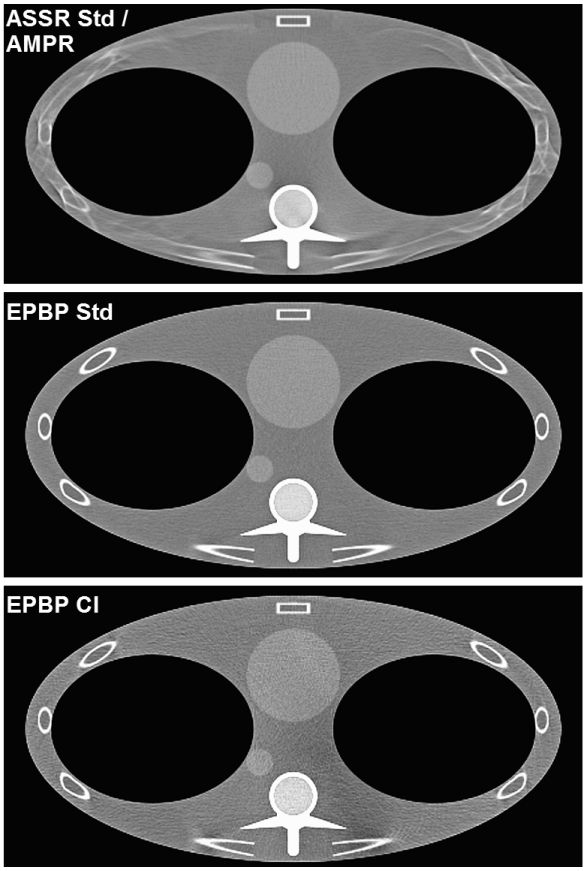

Fig. 1. Thorax, scanned with 256 × 0.75 mm collimation and d = 72 mm table increment. A heart rate of 120 min^{-1} was simulated for EPBP CI. (0/500)

Considering that EPBP CI uses only a fraction of the data available (here, roughly 25%), depending on the local heart rate and on the reconstruction position, the images are almost as good as the EPBP Std reconstructions, apart from the increased image noise. The only exception is a slight variation in the reconstructed density close to the vertebrae.

Figure 2 shows reconstructions of the cardiac motion phantom for a 16–slice and a 256–slice scanner. Since the

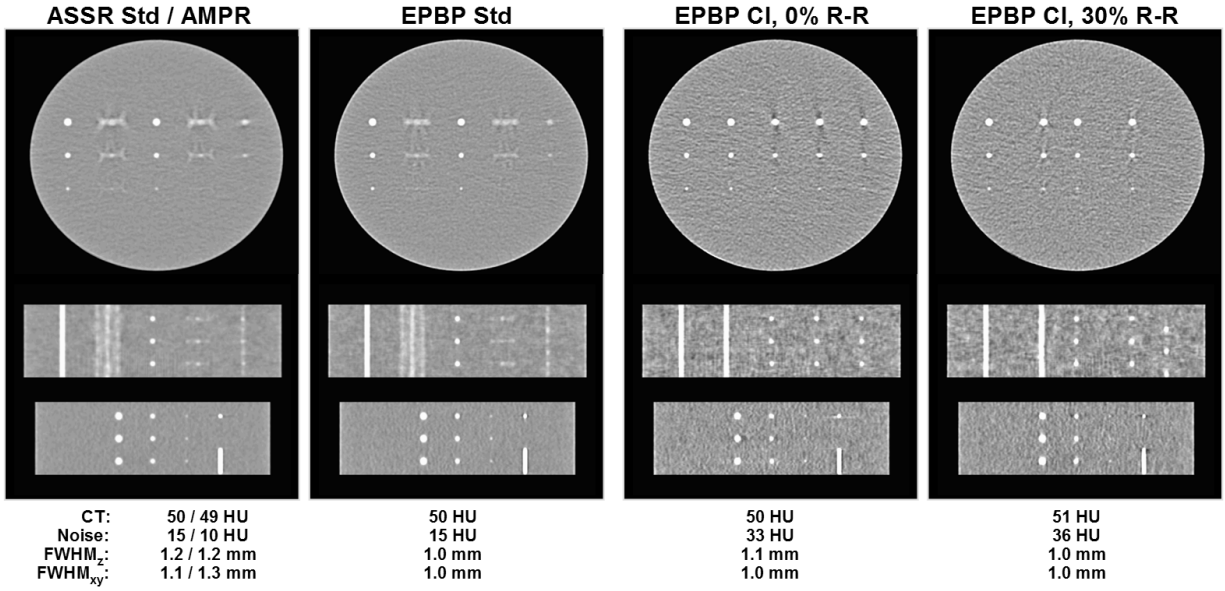

(a)16 × 0.75 mm collimation

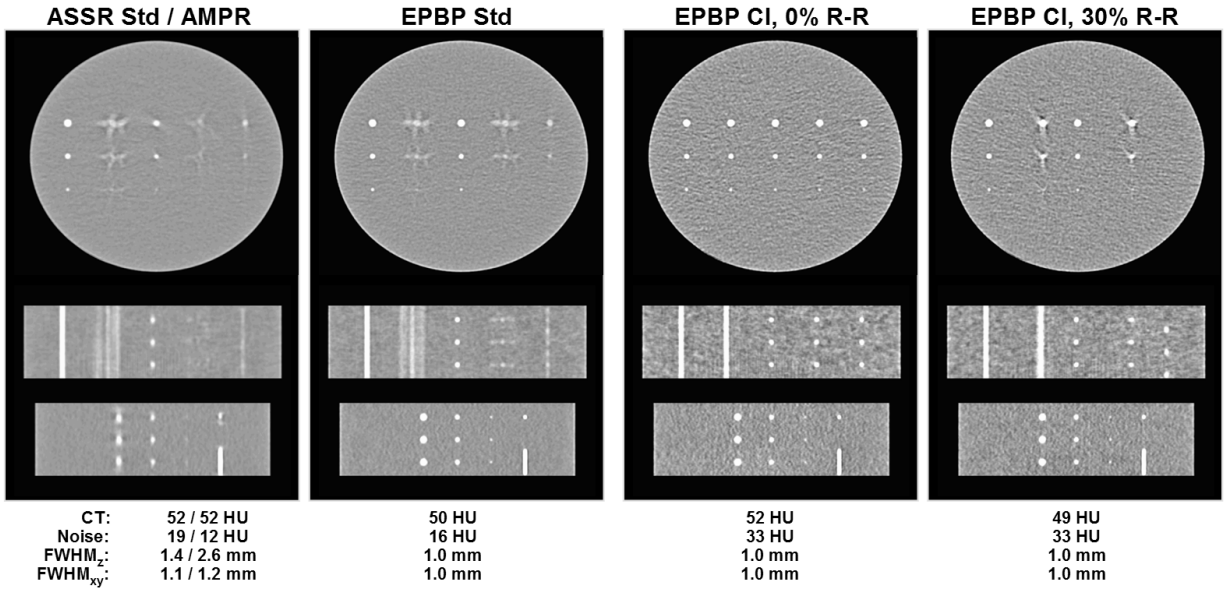

(b)256 × 0.75 mm collimation

Fig. 2. Transaxial slices and MPRs of the cardiac motion phantom reconstructed with various algorithms using a standard 16–slice scanner and a wide cone–angle 256–slice CT. The sagittal MPRs (bottom) show additional δ–objects used to measure resolution. (0/500)

field of view shows only the central parts of the patient, the in–plane images of the ASSR approach are acceptable even for the 256–slice scanner. However, with 256–slice ASSR the multiplanar reformations (MPRs) tend to be blurred in the z–direction and full width at half maximum FWHM_z of the slice sensitivity profile is increased significantly whereas the in–plane resolution FWHM_{xy} is the same as for the 16–slice case.

EPBP, in contrast, behaves very well for all simulated scanners (16, 32, 64, 128 and 256 slices). Spatial resolution is slightly higher than for the single–slice rebinning algorithms. Image noise increases for EPBP CI due to the phase–weighting. This observation is valid for all the other simulated geometries and heart rates (we have looked into $f_\mathrm{H} = 40\ \mathrm{min}^{-1}, \ldots, 140\ \mathrm{min}^{-1}$). EPBP generally behaves equal to or better than ASSR.

Finally, figure 3 gives an example of reconstructed patient data. The data shown are correlated to the patient motion function, the so–called kymogram, which can directly be derived from the acquired rawdata [12]. The standard reconstructions of ASSR Std and EPBP Std are comparable due to the low number of slices; the phase–correlated EPBP CI images are of high image quality and correspond to the gold–standard in cardiac CT imaging.

VI. Discussion

The extended parallel backprojection appears to be adequate for medical CT image reconstruction in all respects. EPBP image quality is equivalent to existing 4– or 16–slice standard and cardiac algorithms for a wide range of

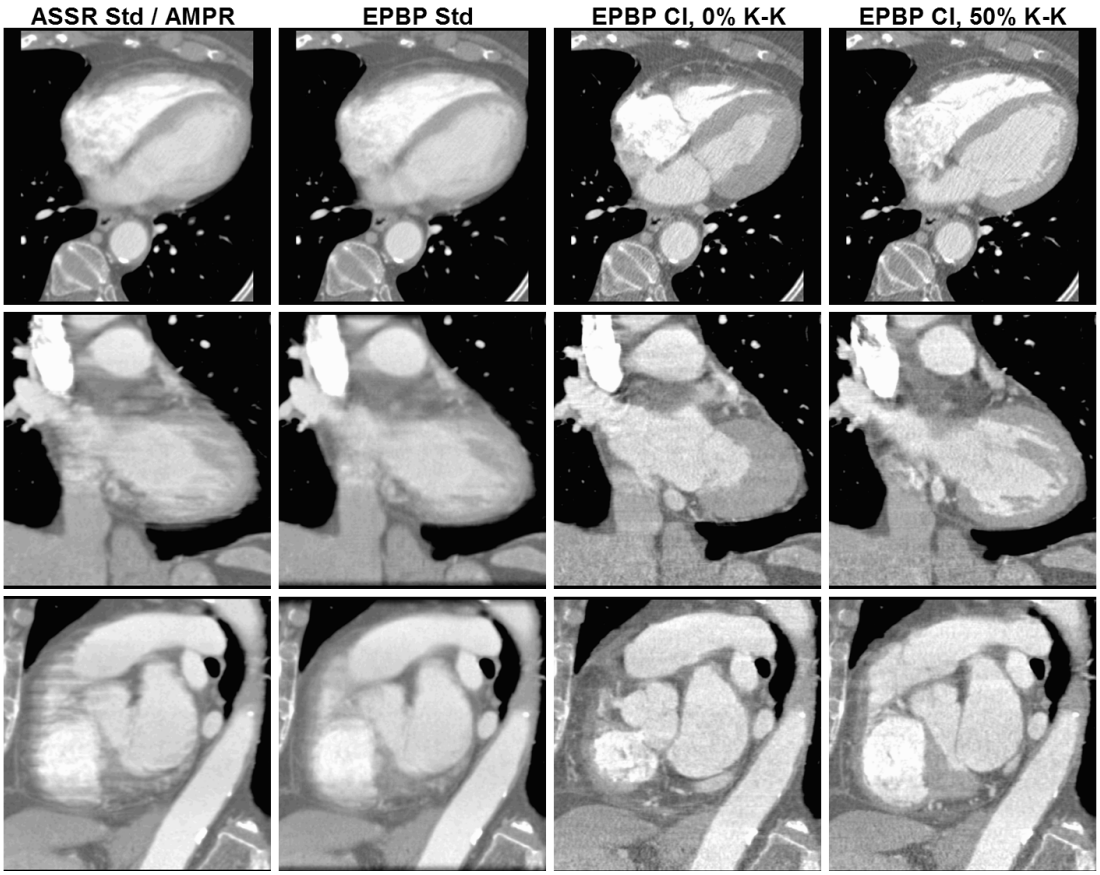

Fig. 3. ASSR and EPBP, 12×0.75 mm collimation, 3.375 mm table increment. The phase–correlated images are reconstructed relative to the kymogram peaks at 0% and 50% of K-K, respectively. (0/500)

simultaneously scanned slices. Even data with $M = 256$ slices yields excellent image quality. For standard reconstructions this is not surprising since EPBP Std is similar to other Feldkamp algorithms (as long as these perform convolution along the tangent direction). For wide cone angle cardiac data, where no other phase–correlated cone–beam algorithm is available yet, EPBP CI performs very well even for objects far off the isocenter (ribs in figure 1).

Feldkamp–type algorithms are superior to ASSR [2], AMPR [11], or SMPR [9] for large M. Wide cone angle cardiac CT is currently only possible with EPBP. Its unique weighting strategy that assigns individual data ranges to each voxel, ensures 100% data usage and thus the maximum dose utilization possible. The future of medical sequential and spiral CT will certainly include the idea of phase–correlated/phase–weighted 3D backprojection of EPBP–type, or modifications thereof.

References

[1] W. A. Kalender, *Computed Tomography*. Wiley & Sons, 2003.

[2] M. Kachelrieß, S. Schaller, and W. A. Kalender, "Advanced single–slice rebinning in cone–beam spiral CT," *Med. Phys.*, vol. 27, pp. 754–772, Apr. 2000.

[3] M. Kachelrieß, T. Fuchs, R. Lapp, D.-A. Sennst, S. Schaller, and W. Kalender, "Image to volume weighting generalized ASSR for arbitrary pitch 3D and phase–correlated 4D spiral cone–beam CT reconstruction," *Proc. of the 6th Int. Meeting on Fully 3D Image Reconstruction*, pp. 179–182, Nov. 2001.

[4] M. Kachelrieß and W. A. Kalender, "Extended parallel backprojection for cardiac cone–beam CT for up to 128 slices," *Radiology*, vol. 225(P), p. 310, Nov. 2002.

[5] M. Kachelrieß and W. A. Kalender, "ECG–based phase–oriented image reconstruction from subsecond spiral CT scans of the heart," *Radiology*, vol. 205(P), p. 215, Nov. 1997.

[6] M. Kachelrieß and W. A. Kalender, "Electrocardiogram–correlated image reconstruction from subsecond spiral computed tomography scans of the heart," *Med. Phys.*, vol. 25, pp. 2417–2431, Dec. 1998.

[7] M. Kachelrieß, S. Ulzheimer, and W. A. Kalender, "ECG–correlated image reconstruction from subsecond multi–slice spiral CT scans of the heart," *Med. Phys.*, vol. 27, pp. 1881–1902, Aug. 2000.

[8] M. Kachelrieß, S. Ulzheimer, and W. A. Kalender, "ECG–correlated imaging of the heart with subsecond multislice CT," *IEEE Transactions on Medical Imaging*, vol. 19, pp. 888–901, Sept. 2000.

[9] K. Stierstorfer, T. Flohr, and H. Bruder, "Segmented multiple plane reconstruction – a novel approximate reconstruction for multi–slice spiral CT," *Phys. Med. Biol.*, vol. 47, pp. 2571–2851, 2002.

[10] K. Sourbelle, *Performance Evaluation of Exact and Approximate Cone–Beam Algorithms in Spiral Computed Tomography*. PhD Thesis, Friedrich–Alexander–Universität Erlangen–Nürnberg, 2002.

[11] S. Schaller, K. Stierstorfer, H. Bruder, M. Kachelrieß, and T. Flohr, "Novel approximate approach for high-quality image reconstruction in helical cone beam CT at arbitrary pitch," *SPIE Medical Imaging Conference Proc.*, vol. 4322, pp. 113–127, 2001.

[12] M. Kachelrieß, D.-A. Sennst, W. Maxlmoser, and W. A. Kalender, "Kymogram detection and kymogram–correlated image reconstruction from subsecond spiral computed tomography scans of the heart," *Med. Phys.*, vol. 29, pp. 1489–1503, July 2002.